Nanoscale

Accepted Manuscript

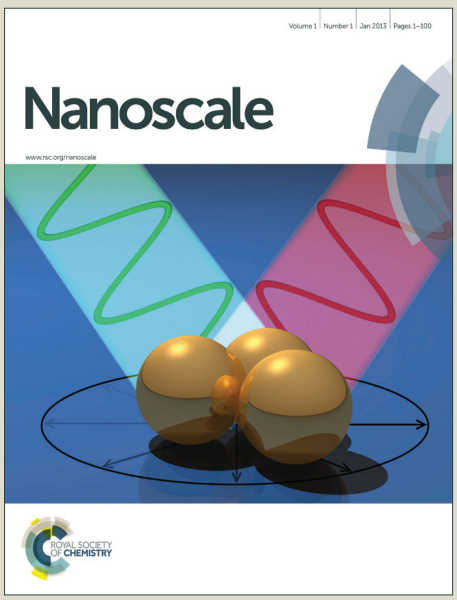

ROYAL SOCIETY OF CHEMISTRY

www.rsc.org/nanoscale

A graphical and textual abstract for the Table of contents entry

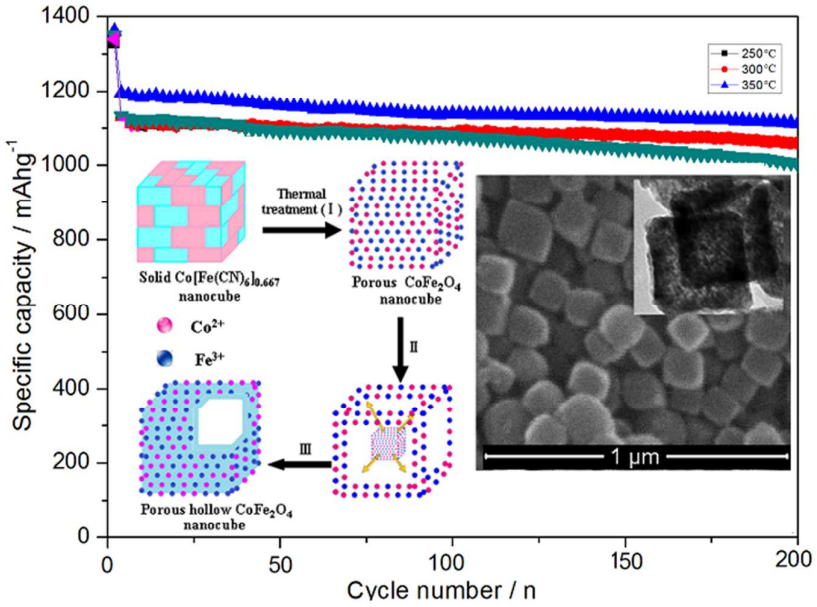

A facile generic environmental strategy is employed to prepare hollow porous $CoFe_2O_4$ nanocubes via metal-organic frameworks. The intrinsic hollow nature as well as the multi-elements characteristics of active components of the unique nanostructures contributes greatly to the outstanding electrochemical performance.

Journal Name

RSCPublishing

ARTICLE

General design of hollow porous $CoFe_2O_4$ nanocubes from metal-organic frameworks with extraordinarily lithium storage

Cite this: DOI: 10.1039/xoxxooooox

Received ooth January 2012,
Accepted ooth January 2012

DOI: 10.1039/xoxxooooox

www.rsc.org/

Hong Guo*, Tingting Li, Weiwei Chen, Lixiang Liu, XiangjunYang*, Yapeng Wang and Yicheng Guo

Hollow porous $CoFe_2O_4$ nanocubes from metal-organic frameworks are fabricated through a general facile strategy. The intrinsic hollow nanostructure can shorten the lengths for both electronic and ionic transport, enlarge the surface areas of electrodes, and the improve accommodation of the volume change during Li insertion/extraction cycling. The hybrid multi-elements characteristics allow the volume change to take place in a stepwise manner during electrochemical cycle. Therefore, as-prepared $CoFe_2O_4$ electrode exhibits outstanding performance as anode materials for lithium ion batteries. The stable capacity arrives at 815 $mAhg^{-1}$ for 20 C. Subsequently, a specific capacity of ca. 1043 $mAhg^{-1}$ is recovered when the current rate reduces back to 1 C after 200 cycles. This general strategy may shed light on a new avenue for large-scale synthesis of hollow porous hybrid nanocubes via MOFs for energy storage, environmental remediation and other novel applications.

Introduction

Morphology-specific nano/micro-materials have attracted much attention because of their application in the fields of energy storage conversion, environmental remediation, catalysis, drug delivery and various new applications.[1-4] As one type of promising architecture, hollow nanostructures with well-defined interior voids, a large surface area, abundant active sites for reaction, accommodate volume change without pulverizing compared with that of solid counterparts of the same size, have been investigated for a long time.[5-9] Precise control of the size, morphology, composition, crystallinity and building blocks of these hollow architectures can tune their fascinating properties of chemistry and physics as desired effectively, and thus is one of key tasks of modern science and technology. For instance, TiO_2 based hollow materials with different size and morphologies have enhanced photocatalytic and electrochemical properties.[7,10-11] Our previous prepared hollow cage-bell Ag@TiO_2 materials exhibit enhanced lithium-ion storage.[12] Lou and co-workers synthesized coaxial SnO_2@carbon hollow nanospheres for highly reversible lithium storage.[13,14] Up to now, general synthesis of hollow structures involve the growth of desirable shells with the assistance of removable or sacrificial templates such as polymer spheres,[12,15] silica,[16,17] carbon,[18,19] or soft templates such as microemulsion droplets,[12] ionic liquids,[20] and bubbles,[21] and most of the available hollow materials synthesized by multistep template routes above only exhibit relatively simple configurations, such as single-shell particles of one composition. However, most recently, the novel hybrid hollow materials containing multiple layers of shells or multiple compositions exhibit desirable applications and maximize the structural advantages compared to single component hollow structures.[12,19,22-24] Especially, hollow porous hybrid micro/nano-structures exhibit considerable application in both fundamental research and practical applications due to their unique properties. Therefore, a general approach to rationally fabricate hierarchical hollow hybrid nanomaterials is still lacking and it is desirable to obtain these materials through more general, facile and environment-friendly process.

Metal-organic frameworks (MOFs), a new class of organic-inorganic hybrid functional materials with high porosity, large surface area and morphology can be easily tuned upon selection of different metal ions and organic bridging ligands.[7,10,11] Especially, a new burgeoning direction in the field of nano MOFs (NMOFs) is their use as 'precursors' of new nanostructured materials, primarily via a thermolysis procedure. As compared to other templates/precursors, NMOFs offer distinct advantages because of their unique structure and porosity or hollow structures, which provide a tremendous opportunity to develop a series of highly tailorable functional nanomaterials for their possible applications. Most importantly, these NMOFs derived metal oxides exhibit enhanced electrochemical performance when evaluated as anode materials for LIBs.[25] Very recently, our group and others have successfully fabricated the nonspherical hollow structure with porous shells.[26,27] For instance, Stephen Mann et al. reported the synthesis of CuO/Cu_2O composite hollow microspheres.[28] Lou et al. prepared Fe_2O_3 microboxes with hierarchical structured shells simply via annealing Prussian blue (PB)

microcubes in air. Yamauchi et al. reported iron oxides with hollow interiors obtained by calcination of PB hollow nanoparticles.[29] Jaephil Cho et al. reported the spindle-like porous α-Fe_2O_3 prepared from a typical iron-based MOFs template (MIL-88-Fe).[30] In this NMOFs templated solid-solid transformation process, noticeably, calcination conditions (e.g., temperature and atmosphere) significantly influence the structure and composition of as-obtained porous products. Unfortunately, in this aspect, it is still a lack of insightful and systematic study. Besides, to our best knowledge, reports on the general synthesis of inorganic functional materials derived from NMOFs and their applications in energy conversion and storage are still at its very early stage, and it can be an advantage for chemists to elaborate possible new constructions from all chemical components without any time-restricted conditions.

Herein, we chose Co-Fe-O hybrid nanostructure to demonstrate our concept and propose a general strategy to prepare hollow porous nanocube structures from NMOFs as **Scheme 1**.

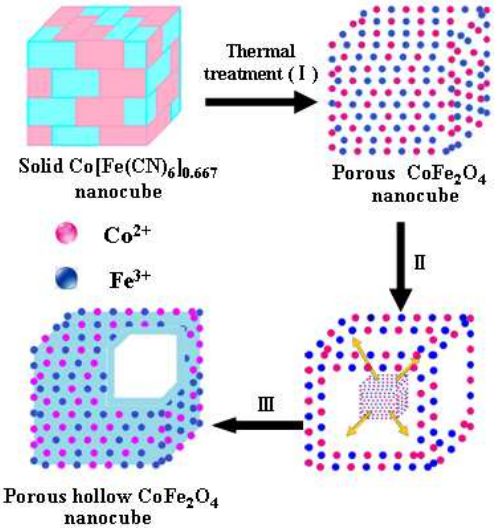

Scheme 1. Representative illustration of the formation of hollow $CoFe_2O_4$ nanocubes from NMOFs.

Transition metal oxides (TMO), especially Fe and Co, have attracted considerable interest as high capacity anode materials for LIBs because of their low cost, non-toxicity and natural abundance.[25,29,30] Nevertheless, the pulverization of the electrode caused by the huge volume changes that occur during the lithiation and delithiation process, makes TMOs exhibit rapid capacity degradation and poor cycling stability. To solve this problem, allowing the electrochemical reaction to proceed in a hybrid matrix of distinct material systems, such as ternary metal oxides with two different metal cations, is an effective way to control the volume changes. In this case, the confining matrix, which can be either active or inactive towards lithium, may be results in the volume change occurs in a step-wise manner rather than at a certain fixed potential, and thus the unreacted component can accommodate the strain yielded by the reacted phase. Furthermore, the coupling of two metal species could render the TMOs with rich redox reactions and improve electronic conductivity. As a result, ternary $CoFe_2O_4$ exhibits higher electrical conductivity and improves electrochemical activity compared with binary metal oxides Fe_2O_3 and Co_3O_4.[27] Another popular way to improve the electrochemical performance of TMOs has been focused on controlling the volumetric change by using small particles with various morphologies, of which hollow particles are of particular interest for reversible lithium ion storage because of their short Li^+ diffusion and good toleration for volume change during cycling.[12-14,25-27] Though these procedures are effective, each designed strategy alone always leads to limited improvement in the electrochemical properties of TMOs. In this work, the advantage of novel hollow nanocube structures from NMOFs and the virtue of hybrid matrix of distinct material systems are well integrated to solve the problem. As a result, the geometric configuration and outstanding electrochemical performance of hierarchical hollow $CoFe_2O_4$ nanocubes from metal-organic frameworks are anticipated to manifest outstanding electrochemical performance.

Experimental

Synthesis of solid $Co[Fe(CN)_6]_{0.667}$ nanocubes

All chemicals were of analytical grade and used without further purification. In a typical procedure, $K_3[Fe(CN)_6]$ (2 mmol) and 100 mL of aqueous solution of $Co(CH_3COO)_2$ (1 mmol) was added into 100 mL of aqueous solution of PVP K30 (4 g) under stirring, after 10 min a burgundy turbid liquid was formed and then aged for 24 h. The above reaction is conducted at room temperature. The resulting burgundy product was harvested by several rinse-precipitation cycles with deionized (DI) water for further characterization.

Synthesis of hollow porous $CoFe_2O_4$ nanocubes

Certain amount of $Co[Fe(CN)_6]_{0.667}$ precursors were successively annealed in Air flowing at 350 °C for 4 h with a slow ramp rate of 1 °C min^{-1} to make hollow porous $CoFe_2O_4$ nanocubes.

Characterization

X-ray diffraction (XRD) was carried out to identify the phase composition of synthesized samples over the 2θ range from 3° to 90° using a Rigaku D/max-A diffractometer with Co Kα radiation. A Fourier transform infrared spectroscope (FTIR, Themo Nicolet 670FT-IR) was used for recording the FTIR spectra of the sample ranging from 400 to 4000 cm^{-1}. Morphologies of the synthesized samples were observed with a AMRAY 1000B scanning electron microscope (SEM), and the microstructural characteristics of samples were observed by high-resolution transmission electron microscope (HR-TEM, JEOL JEM-2010) working at 200 kV accelerating voltage and the lattice structure was identified by selected area electron diffraction (SAED) technique. Nitrogen adsorption-desorption measurements were conducted at 77 K on a Micromeritics Tristar apparatus. Specific surface areas were determined following the Brunauer-Emmet-Teller analysis.

Electrochemical Measurements

For electrochemical performance evaluation, half-cell studies were performed. In the experimental electrode, acetylene black powder and polyvinylidene fluoride (PVDF) were used as conductive additive and binder. The synthesized active materials were mixed with acetylene black and PVDF dissolved in N-methyl-pyrrolidinone in the weight ratio of 80:10:10 to form slurry, which was painted on a copper foil used as current collector. After solvent evaporation, the electrode was pressed and dried at 120 °C under vacuum for 48 h. The cells were assembled in argon filled glove-box. Metallic lithium foil was used as counter electrode. The electrolyte was 1M $LiPF_6$ in a mixture of ethylene carbonate (EC) and dimethyl carbonate (DMC) (1:1 in vol. ratio). Cycling tests were carried out at the charge and discharge density of 1 C, 5 C, 10 C and 20 C, in the voltage range of 0.01-3.0 V versus Li/Li^+ by Land 2100A

tester. Cyclic voltammetry was performed between 0.01 and 3.0 V with scan rate of 0.01 mVs^{-1}.

Results and discussion

The crystallographic structure and phase purity of the precursor and as-synthesized hollow porous $CoFe_2O_4$ nanocubes are analysed by XRD, as shown in Fig. 1a and b. The precursor can be identified as $Co[Fe(CN)_6]_{0.667}$ (JCPDS card no. 86-0502) without impurit ies as shown in Fig. 1a. All the diffraction peaks of final products can be indexed to the monoclinic phase of $CoFe_2O_4$ (JCPDS card no. 22-1086). No other impurity peaks are observed, indicating a complete thermal conversion of the MOF precursors into $CoFe_2O_4$ nanostructures. Detailed analysis of the peak broadening of the (3 1 1) reflection of $CoFe_2O_4$ using the Scherrer equation indicates an average crystallite size ca. 8 nm, suggesting that these particles are composed of nanocrystal subunits. 8% (wt.%) carbon is remained in the composite by TG analysis (Fig. S1).

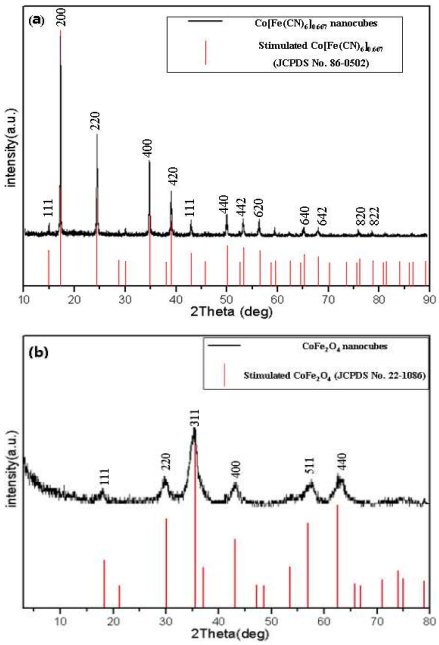

Fig. 1 XRD pattern of hollow $CoFe_2O_4$ nanocubes (b) and its precursor of $Co[Fe(CN)_6]_{0.667}$ (a).

The FTIR spectrum images of the prepared hollow structured $CoFe_2O_4$ nanocubes sample and its $Co[Fe(CN)_6]_{0.667}$ precursor are shown in Fig. S2. The broad absorption peaks centered at ca. 3419 to 2349 cm^{-1} are associated with the stretching vibrations of the -OH group of absorbed water molecules and absorption of CO_2 in the air. According to the spectrum of $Co[Fe(CN)_6]_{0.667}$, those peaks from 1646 to 1608 cm^{-1} are assigned to the bending vibrations of the water molecules; the spikes from 2155 to 2110 cm^{-1} are assigned to the stretching vibrations of the cyano group of precursor. These peaks disappeared in the spectrum of synthesized $CoFe_2O_4$ samples, indicating these groups have decomposed after calcinations. The strongest broad peaks in the range of 1041 to 400 cm^{-1} are contributed from the face-centered spinel structural phase Fe-O. The peak intensity of Fe-O bond for $CoFe_2O_4$ products is different from that of precursor, implying the structure of prepared sample has some discrepancy with its precursor.

The SEM and TEM images of the prepared $Co[Fe(CN)_6]_{0.667}$ precursors are shown as Fig. 2a and b. It is obvious that the precursors are solid submicro-cubes uniformly with average diameter of ca.100 nm according to Fig. 2a. TEM (Fig. 2b) reveals that these solid submicro-cubes have a smooth surface. The unique hollow porous morphology of $CoFe_2O_4$ nanocube sample is also characterized by SEM, TEM and HR-TEM, as illustrated in Fig. 1c-f. After calcining the $Co[Fe(CN)_6]_{0.667}$ precursors at 350 °C for 4 h, a fluffy black powder is obtained and the size have a little shrunk compared with its precursors as presented in Fig. 2c, illuminating the products are uniform cube shape. It is interesting to find that the $CoFe_2O_4$ sample from MOFs is not a solid box but a visible hollow porous interior structure with average diameter of ca. 80 nm obviously, as evidenced by the partial broken shell vividly according to Fig. 2d. Especially, a typical structure with well-defined interior and very thin shell can also be detected. Furthermore, the surface of samples exhibits porous frame, which hierarchical structure is resulted from MOFs. The size of as-synthesized nanocubes is much smaller than those reported by Lou very most recently.[31] The hollow porous structure of these particles might be caused by rapid mass-transport across the shells during calcinations. The surface of the synthesized $CoFe_2O_4$ powder is made up from nano-sized small particles of ca. 3-9 nm, which is in good agreement with XRD results. Its selected-area electron diffraction (SAED) pattern (Fig. 2e) reveals the diffraction rings 1-3 are indexed to (2 2 0), (3 1 1), and (4 0 0) diffraction of face-centered cubic NiO, respectively. The lattice fringe is observed obviously, and the lattice spacing (0.251 nm) agrees with $CoFe_2O_4$ (3 1 1) plane spacing from Fig. 2f.

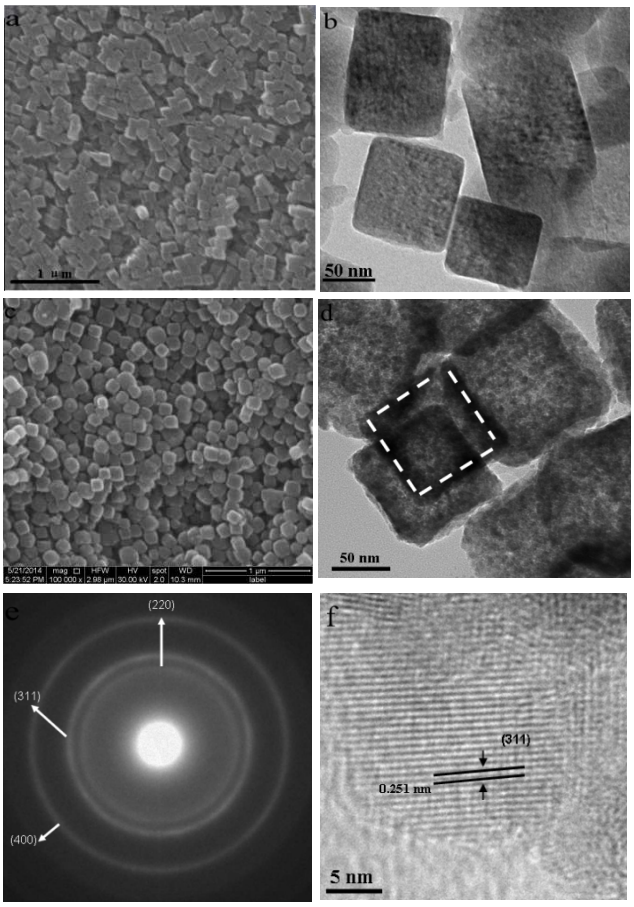

Fig. 2 SEM (a) image and TEM (b) image of as-prepared $Co[Fe(CN)_6]_{0.667}$ nanocubes precursor; SEM image (c), TEM (d) image, selected area electron diffraction (SAED) (e) and HRTEM micrographs (f) of as-synthesized hollow $CoFe_2O_4$ nanocubes yielded by calcinations at 350 °C.

The N_2 adsorption/desorption isotherms and the pore size distribution of the obtained hollow porous $CoFe_2O_4$ nanocubes from MOFs are shown as Fig. 3. The isotherms are identified as type IV, which are the characteristic isotherm of mesoporous materials. The pore size distribution data indicates that average pore diameters of the product are in the range of 3-8 nm. The BET surface area of the sample is 102.692 m^2 g^{-1}. Remarkably, the specific surface area of $CoFe_2O_4$ is far higher than most of the previous reported TMOs microsphere products.[27, 30, 31] The single-point total volume of pores at P/P_0 = 0.975 is 0.438 cm^3 g^{-1}. These indicate that the prepared samples have a loose mesoporous structure. This structure not only can keep the nano effect of active components but also help to buffer the volume changes of hollow porous $CoFe_2O_4$ nanocube electrodes during electrochemical reaction.

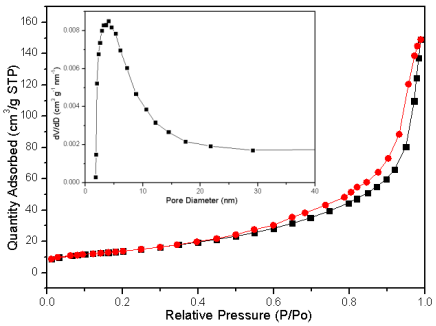

Fig. 3 N_2 adsorption/desorption isotherm (77K) curve for hollow $CoFe_2O_4$ nanocubes (350 °C). Inset: The pore-size distribution of the $CoFe_2O_4$ nanocubes.

The formation mechanism can be described as schematically illustrated in Scheme 1 by the following Equation (1). When $Co[Fe(CN)_6]_{0.667}$ was converted into $CoFe_2O_4$, the carbon and nitrogen in CN^- were oxidized into gases and escaped.

$$Co[Fe(CN)_6]_{0.667} + O_2 = CoFe_2O_4 + CO_2 + N_xO_y + H_2O \quad (1)$$

The formation mechanism is tracked to investigate according to Fig. 4, which is TEM images of $CoFe_2O_4$ calcination at 200 °C, 250 °C, 300 °C, 350 °C, 400 °C and 450 °C for 4 h. It is found that only solid nanocubes with a smooth surface formed after calcination at 200 °C (Fig. 4a). When the temperature is increased at 250 °C, the surface of sample becomes a little coarse and show porous structure (Fig. 4b). Then its surface becomes more coarse and the hollow configure is visible gradually with the increase of reaction temperature (Fig. 4c, 300 °C). It is significant noticed that the porous nanocubes transformed into hollow ones while the temperature arrived at 350 °C (Fig. 4d). Further increasing the temperature, the interior of the nanocube structures are broken and become small nano particles of ca.4-8 nm as Fig. 4e and f corresponding to 400 °C and 450 °C, respectively. According to above experiments, it can be speculated that the formation of the unique hollow porous $CoFe_2O_4$ nanocubes go through the transformation of the solid to hollow ones, which can be attributed to that the CO_2 and N_xO_y gases are released quickly during the thermal decomposition process and the porous nanocubes collapse as the temperature increased. Liu recently demonstrated a general top-down thermal oxidation strategy for the synthesis of uniform porous transition-metal oxide hollow capsules based on the Kirkendall effect of inorganic materials.[32] However, there are few reports on the Kirkendall effect of coordination compounds, such as PBA system of $Co[Fe(CN)_6]_x$. Therefore, our research on Kirkendall effect of PBA $Co[Fe(CN)_6]_x$ may complement the current knowledge in modern science and technology. On the basis of the above analysis, Scheme 1 of the process for the preparation of $CoFe_2O_4$ hollow porous nanocubes is reasonable. Our strategy provides a novel general route to prepare hierarchical hollow porous nanocubes from MOFs with simpler route, higher BET surface and larger quantity. This strategy can also be used to prepare other nano/micro-cube advanced materials, such as $NiFe_2O_4$ (Fig. S3) $ZnCo_2O_4$ (Fig. S4) and $NiCo_2O_4$ (Fig. S5), for details see supporting information.

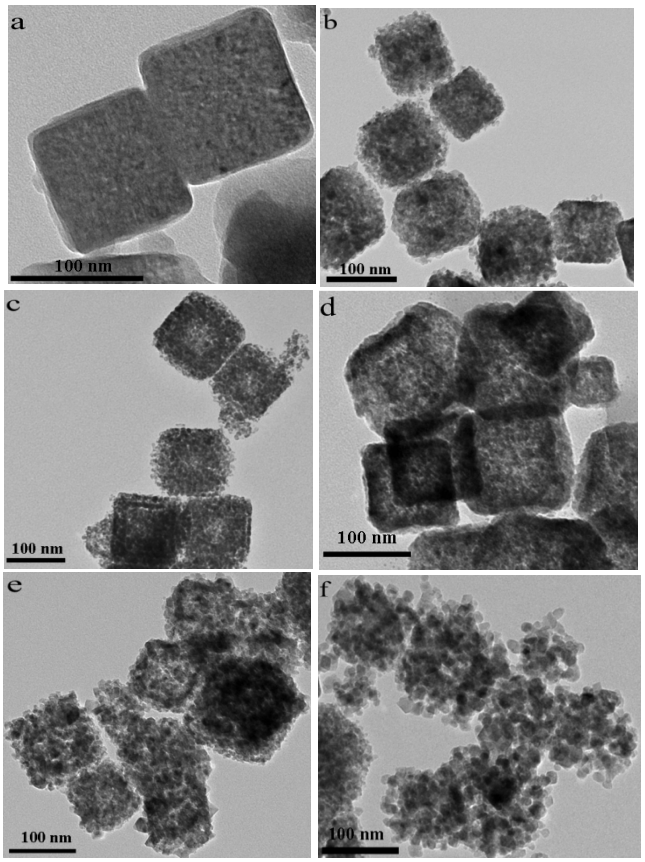

Fig. 4 TEM images of porous $CoFe_2O_4$ nanocubes obtained at (a) 200 °C, (b) 250 °C, (c) 300 °C, (d) 350 °C, (e) 400 °C, (f) 450 °C for 4 h.

The electrochemical performance of the prepared hollow $CoFe_2O_4$ nanocubes used for Li-ion anodic materials is investigated. According to Fig. 5a, the increase in cycling stability and capacity with the increase of temperature from 250 °C to 350 °C is mainly attributed to the formation of hollow porous structure. The capacity of the sample of 350 °C can remain stable as high as 1115 $mAhg^{-1}$ after 200 cycles with a little higher than that of 300 °C. However, when the temperature rises to 450 °C, its capacity fades drastically from 1340 to 765 $mAhg^{-1}$ after 200 cycles. This result is understandable because of the hollow structures are destroyed in the process of calcination at high temperature as evidenced in Fig. 4 above. The cycle of CV curves and charge/discharge of hierarchical hollow porous $CoFe_2O_4$ nanocube (350 °C) electrode are shown in Fig. 5b and c, respectively. In the first scan of CV, two cathodic peaks are observed at 0.54 and 1.45 V, corresponding to the conversion reactions of Fe^{3+} and Co^{2+} to their metallic states and the formation of Li_2O.[33] The broad anodic peak for both can be ascribed to the oxidation reactions of metallic Fe and Co. The reaction of $CoFe_2O_4$ with Li can be written as Equation (2):

$$CoFe_2O_4 + 8Li^+ + 8e^- = 2Fe + Co + 4Li_2O \quad (2)$$

Similar to the simple oxide CoO and NiO, the mixed oxide $CoFe_2O_4$ stores Li through reversible formation and decomposition of Li_2O. In the second scan, the reduction peaks are shifted to 0.70 and 1.51 V. The asymmetric nature of the plots suggests that the conversion reactions are only partially reversible and complete structural recovery to $CoFe_2O_4$ cannot occur.[34] According to the 1st, 2nd, and 200th discharge (Li^+ insertion) and charge (Li^+ extraction) curves at a current density of 1 C in the voltage window of 0.01-3 V (Fig. 3c). There is a wide, steady discharging plateau at ca. 1.0 V in the first cycle, followed by a gradual voltage decrease. The initial discharge and charge capacities are 1352 $mAhg^{-1}$ and 1190 $mAhg^{-1}$, respectively. The initial capacity loss should be attributed to the formation of solid electrolyte interphase (SEI) and the reduction of metal oxide to metal with Li_2O formation. The initial coulombic efficiency is 85.3%, which is lower than most reported TMOs electrodes.[34-36] These results are consistent with CV analysis. From the second cycle onwards, the long potential plateau was replaced by a long slope between 1.5 and 0.75 V. After 200 cycles, the capacity can also be kept at 1115 $mAhg^{-1}$, showing the excellent reversibility of electrode. To investigate electrochemistry performance under the different rate discharge, Fig. 5d exhibits the discharge capacities of $CoFe_2O_4$ electrode against different current rates from 1 C to 20 C, and each sustained for 40 cycles. The stable cyclic performance is obtained for all rates. Even when the current reaches 20 C, the capacity can also arrive at 815 $mAhg^{-1}$. Subsequently, a specific capacity of ca. 1043 $mAhg^{-1}$ is recovered when the current rate reduces back to 1 C after 200 cycles. The overall rate performance demonstrates the high capacities in both low and high current rates of the hollow porous $CoFe_2O_4$ nanocube electrode.

Fig. 6 is the TEM of $CoFe_2O_4$ electrode after 200 cycles at current density of 1 C, revealing materials is still kept well without breakage in the process of charge-discharge. Compared with the previous reported TMOs materials,[25,27,35-40] the material reported here is very attractive due to its facile, fast, and improved lithium storage. The nano-scaled characteristics of $CoFe_2O_4$ particle from MOFs embedded in the nanocubes ensure the electrode having a high capacity and the fast Li-ion diffusion in the electrode, and the introduction of carbon renders the electrode having a good electronic conductivity. The unique hollow porous nanocube structures can shorten the length of Li-ion diffusion, which is benefit for the rate performance. Besides, the hollow structure offers a sufficient void space, which sufficiently alleviates the mechanical stress caused by volume change. The multi-elements characteristics allow the volume change to take place in a stepwise manner during electrochemical cycle. Therefore, the hierarchical hollow $CoFe_2O_4$ nanocube electrode exhibits outstanding electrochemical performance.

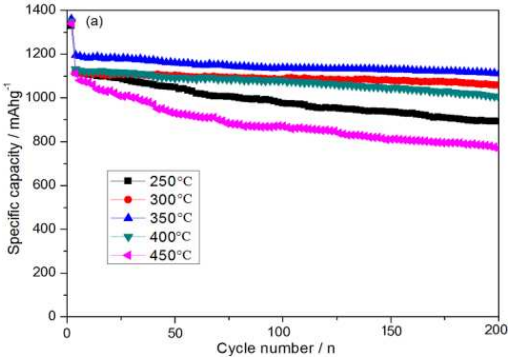

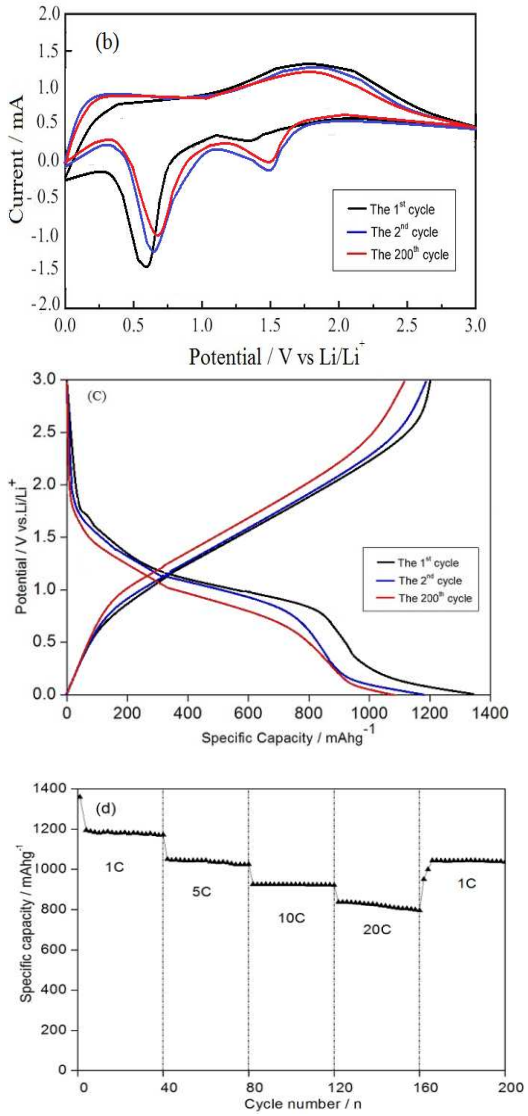

Fig. 5 Electrochemical performance of prepared hierarchical porous hollow $CoFe_2O_4$ nanocube electrode: (a) cycling performance of $CoFe_2O_4$ materials at different temperatures from 250 °C to 450 °C at constant current density of 1 C; b) the cycle of CV curve with a scan rate of 0.05 mVs^{-1}; (c) charge/discharge curves of $CoFe_2O_4$ (350 °C) electrode for the 1st, 2nd, and 200th cycle at current density of 1 C; (c) the first cycle CV curve with a scan rate of 0.05 mVs^{-1}; (d) rate capability of $CoFe_2O_4$ electrode from 1 C to 20 C for 200 cycles. Electrode potential range of 0.01-3.0 V vs. Li/Li^+.

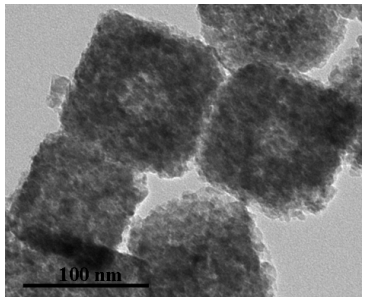

Fig. 6 TEM image of hybrid yolk-shell structured $CoFe_2O_4$ electrodes after 200 cycles at 1C.

Conclusions

In summary, hollow porous $CoFe_2O_4$ nanocube electrodes from MOFs are successfully synthesized by a facile and fast benign procedure. The stable reversible capacity of electrode can be retained at 1115 $mAhg^{-1}$ after 200 cycles, and it also exhibits excellent rate performance. This general strategy may shed light on a novel avenue for the effective synthesis of hollow porous hybrid nanocube materials derived from MOFs for energy storage, sensor, catalyst, environmental remediation and other new applications.

Acknowledgments

The authors would like to acknowledge financial support provided by the National Natural Science Foundation of China(No.51474191 and No.21467030) and the Major state basic research development program of China (973 Program, No. 2014CB643406).

Notes and references

Hong Guo*, School of Chemistry Science and Engineering, Yunnan University, Kunming 650091, Yunnan, China. Fax: +86-871-65036626; Tel: +86-871-65032180; E-mail: guohongcom@126.com

Xiangjun Yang*, School of Chemistry Science and Engineering, Yunnan University, Kunming 650091, Yunnan, China. E-mail: yxjun622@163.com

Electronic Supplementary Information (ESI) available: [details of any supplementary information available should be included here]. See DOI:10.1039/b000000x/

1 J. Liu, S. Z. Qiao, S. B. Hartono and G. Q. M. Lu, *Angew. Chem.,* 2010, **122**, 5101.
2 B. Wang, J. S. Chen, H. B. Wu, Z. Y. Wang and X. W. Lou, *J. Am. Chem. Soc.,* 2011, **133**, 17146.
3 Z. F. Bian, J. Zhu, J. G. Wang, S. X. Xiao, C. Nuckolls, H. X. Li, *J. Am. Chem. Soc.,* 2012, **134**, 2325.
4 X. W. Lou, C. M. Li and L. A. Archer, *Adv. Mater*., 2009, **21**, 2536.
5 H. Guo, D. Tian, L. Liu, Y. Wang, Y. Guo and X. Yang, *J. Solid State Chem*., 2013, **201**, 137.
6 Y. Yin, R. M. Rioux, C. K. Erdonmez, S. Hughes, S, G. A. Somorjai and A. P. Alivisatos, *Science,* 2004, **304**, 711.
7 L. Liu, Y. Guo, Y. Peng, X. Yang, S. Wang and H. Guo, *Electrochim. Acta,* 2013, **114**, 42.
8 Q. Zhang, I. Lee, J. B. Joo, F. Zaera and Y. Yin, *Acc. Chem. Res.,* 2013, **46**, 1816.
9 Y. Yao, M. T. McDowell and I. Ryu, *Nano lett.,* 2011, **11**, 2949.
10 H. Guo, Y. P. Wang, W. Wang, L. X. Liu, Y. Y. Guo, X. J. Yang and S. X. Wang, *Part. Part. Syst. Charact.,* 2014, **31**,374.
11 X. Lai, J. Li, B. A. Korgel, Z. Dong, Z. Li, F. Su, J. Du and D. Wang, *Angew. Chem. Int. Ed.,* 2011, **50**, 2738.
12 H. Guo, W. Wang, L. Liu, Y. He, C. Li and Y. Wang. *Green Chem.,* 2013, **15**, 2810.
13 L. Zhou, D. Zhao and X. W. Lou, *Adv.Mater.,* 2012, **24**, 745.
14 Z. Wang, Z.Wang, W. Liu, W. Xiao and X. W. Lou, *Energy Environ. Sci.,* 2013, **6**, 87.
15 Z. Peng, J. Wu and H. Yang, *Chem. Mater.,* 2010, **22**, 1098.
16 K. Nelson and Y. Deng, Langmuir, 2008, **24**, 975.
17 D. Wang and H. Zeng, *Chem. Mater.,* 2009, **21**, 4811.
18 Y. Ao, J. Xu, D. Fu and C. Yuan, *Catal. Commun.,* 2008, **9**, 2574.
19 H. Guo, Y. He, Y. Wang, L. Liu, X. Yang, S. Wang, Z. Huang and Q. Wei, *J. Mater. Chem. A,* 2013, **1**, 7494.
20 T. Nakashima and N. Kimizuka, *J. Am. Chem. Soc.,* 2003, **125**, 6386.
21 X. Li, Y. Xiong, Z. Li and Y. Xie, *Inorg. Chem.,* 2006, **45**, 3493.
22 C. Wu, X. Wang and L. Zhao, *Langmuir,* 2010, **26**, 18503.
23 Y. Wang, F. Su and J. Y. Lee, *Chem. Mater*., 2006, **18**, 1347.
24 J. Deng, C. Yan and L. Yang, *Nano,* 2013, **7**, 6948.
25 L. Zhang, H. B. Wu and X. W. Lou, *Adv. Energy Mater.,* 2014**,** DOI:10.1002/aenm.201300958.
26 H. Guo, L. Liu, T. Li, W. Chen, J. Liu, Y. Guo and Y. Guo, *Nanoscale,* 2014, **6**, 5491.
27 L. Hu and Q. Chen, *Nanoscale,* 2014, **6**, 1236.
28 H. G. Yu, J. G. Yu, S. W. Liu and S. Mann, *Chem. Mater.,* 2007, **19**, 4327.
29 M. Hu, A. A. Belik, M. Imura, K. Mibu, Y. Tsujimoto and Y. Yamauchi, *Chem. Mater.,* 2012, **24**, 2698.
30 X. D. Xu, R. G. Cao, S. Jeong and J. Cho, *Nano Lett.,* 2012, **12**, 4988.
31 L. Zhang, H. B. Wu and X. W. Lou, *J. Am. Chem. Soc*., 2013, **135**, 10664.
32 J. Liu and D. E. Xue, *Adv. Mater.,* 2008, **20**, 2622.
33 C. Vidal-Abarca, P. Lavela and J. L. Tirado, *Solid State Ionics,* 2010,**181**, 616.
34 P. Lavela, J. L. Tirado, M. Womes and J. C. Jumas, *J. Phys. Chem. C,* 2009, **113**, 20081.
35 G. Q. Zhang, H. B. Wu, H. E. Hoster, M. B. Chan-Park and X. W. Lou, *Energy Environ. Sci.,* 2012**, 5**, 9453.
36 G. Zhang and X. W. Lou, *Adv. Mater.,* 2013, **25**, 976.
37 H. Jiang, J. Ma and C. Z. Li, *Chem.Commun.,* 2012, **48**, 4465.
38 H. L. Wang, Q. M. Gao and L. Jiang, *Small,* 2011, **7**, 2454.
39 C. Z. Yuan, J. Y. Li, L. R. Hou, L. Yang, L. F. Shen and X. G. Zhang, *J. Mater. Chem.,* 2012, **22**, 16084.
40 L. L. Li, S. J. Peng, Y. L. Cheah, P. F. Teh, J. Wang, G. Wee,Y. W. Ko, C. L. Wong and M. Srinivasan, *Chem. Eur. J.,* 2013, **19**, 5892.

